Effects of End-Wall Opening on Flow in A Ventilated Chamber: A Numerical Study

Suthichock Nunthasookkasame and Asi Bunyajitradulya
Fluid Mechanics Research Laboratory, Department of Mechanical Engineering
Faculty of Engineering, Chulalongkorn University
Bangkok 10330, Thailand
Tel. 0-2218-6645, 0-2218-6647; Fax. 0-2252-2889
Email: basi@chula.ac.th
http://www.eng.chula.ac.th/~fmeabj

Abstract

Effects of end-wall opening on laminar flow in a ventilated chamber at low Reynolds numbers of 1, 10, and 100 are investigated numerically. The two-dimensional chamber is 50 cm high and 100 cm long. The supply inlet with 4 cm height is located on one end-wall immediately under the ceiling and the adjustable outlet is located on the opposite end-wall immediately above the floor. In the calculation, a finite volume method with staggered grid arrangement is used with SIMPLE procedure. The results indicate the followings. At low Reynolds number range, e.g., Re = 1 and 10, Reynolds number affects the flow only in the upstream portion of the chamber while end-wall opening affects the flow only in the downstream portion. In contrast, at higher Reynolds number range, e.g., Re = 100, both Reynolds number and end-wall opening affect the flow throughout the whole chamber. In addition, at high Reynolds number, the flow pattern and characteristics depend on end-wall opening only in the range from 100% (full opening) to approximately 30% opening. On the contrary, in the range of end-wall opening less than 30%, the flow pattern and characteristics are nearly unchanged with end-wall opening. The independence of the flow pattern and characteristics on end-wall opening is found to be associated with the existence of the reattachment-stagnation point of the impinging jet near the end wall and the lack of entrainment of outside fluid into the chamber.

With these results, the physical understanding of the flow in a ventilated chamber is extended further from the study of Stitsuwongkul and Bunyajitradulya (2000). Specifically, the study reveals that the flow pattern and characteristics in a ventilated chamber depend on the end-wall closing only in the range of closing from 0 (fully open) to the end-wall closing characteristic height, δ_c. Beyond δ_c, the flow pattern and characteristics are relatively independent of the closing. In addition, in the range of end-wall closing above δ_c, outside fluid is found to be entrained into the chamber; in contrast, in the range below δ_c, no entrainment is allowed. From physical considerations, it is therefore concluded that δ_c is the closing height that just diverts the ceiling wall jet towards the floor and, as a result, causes the impingement of the jet and the associated reattachment-stagnation point to exist inside the chamber. Equivalently, δ_c is the closing height that just causes the entrainment of outside fluid to stop. Finally, these results suggest that the variation in average temperature with end-wall opening in a ventilated chamber, e.g., in the study of Stitsuwongkul and Bunyajitradulya (2000), is mainly due to the dependency of the entrainment ratio on the opening.

1. Introduction

Flow in a ventilated chamber can be found in many engineering applications. Examples are ventilated/air-conditioned room, storage room, and combustion chamber. In ventilated

RECEIVED 29 JULY, 2002
ACCEPTED 6 MARCH, 2003

chamber, recirculating flow is the main mechanism which affects flow pattern, mixing characteristics, temperature and contaminant distribution, energy consumption, etc. In order to control the pattern and characteristics of the flow in a ventilated chamber, the understanding of the physics of the flow is necessary. Such understanding will lead to better design and control of flow quality in the chamber.

In the literature, there were several works on turbulent flow in a ventilated chamber. However, most of them studied the flow with only one or a few values of opening; examples in this respect are the works of Nielsen et al. (1978), Restivo (1979), Gosman et al. (1980), Davidson and Nielsen (1996), and Davidson (2000). On the other hand, few works addressed the issue of the effects of end-wall opening on flow pattern and characteristics. Examples in this case are the works of Khuhiran et al. (1999), Stitsuwongkul (2000), and Stitsuwongkul and Bunyajitradulya (2000); the latter shall hereafter be referred to as S&B (2000). Because of the importance of the issue in various aspects and in a wide range of engineering applications just as mentioned, the effects of end-wall opening together with the effects of Reynolds number are therefore investigated in this study. The investigation is conducted numerically at low Reynolds numbers of 1, 10, and 100. The ventilated chamber configuration is similar to that of S&B (2000). The results from the two studies are discussed and further characteristics and physics of the flow are extracted.

2. Computational details

The ventilated chamber is two dimensional, 50 cm high (H) and 100 cm long (L). The supply inlet of 4 cm in height (h) is located on one end-wall immediately under the ceiling and the adjustable outlet is located on the opposite end-wall immediately above the floor. The configuration of the chamber is shown in Fig. (1).

The calculations are carried out for steady, incompressible, laminar flow at Re of 1, 10, and 100. The Reynolds number is defined here as $Re = U_{in}h/\nu$, where U_{in} is the uniform velocity at the supply inlet, h is the inlet height and ν is the kinematic viscosity. The effects of end-wall opening are studied by varying the opening ratio (t/H) for 9 values: 1.0 (full opening), 0.92, 0.84, 0.76, 0.68, 0.60, 0.40, 0.20, and 0.08 for all cases, and additional values of opening of 0.96, 0.30, and 0.10 are added to the Re = 100 case.

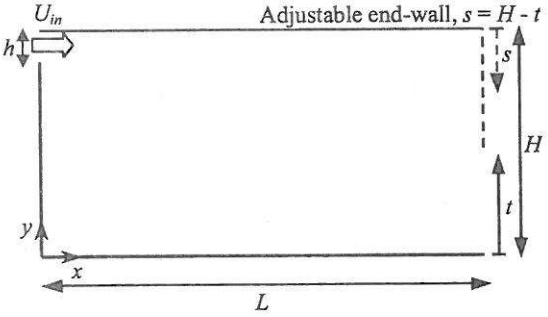

a) Physical domain.

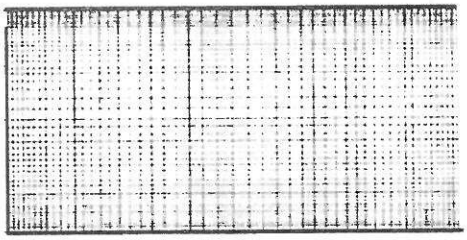

b) Computational domain.

Figure 1. Flow configuration.

For steady incompressible laminar flow, the continuity and the Navier-Stokes equations in Cartesian index notation read

$$\frac{\partial u_i}{\partial x_i} = 0,$$

$$\frac{\partial(\rho u_i u_j)}{\partial x_j} = -\frac{\partial P}{\partial x_i} + \frac{\partial}{\partial x_j}\left(\mu \frac{\partial u_i}{\partial x_j}\right).$$

A steady, incompressible, finite volume code, which is based on SIMPLE algorithm, is used to solve the governing equations. A

staggered-grid arrangement is employed and a second-order central differencing scheme is used to discretize both the convection and the diffusion terms. The code is validated by standard 2D steady state test cases, namely, lid-driven cavity flow and flow through backward facing step. The results show good agreement with previous works of Ghia et al. (1982) and Armaly et al. (1983). Then, grid independence is tested for every opening ratio at the highest Reynolds number on 3 resolutions: 52x52, 102x102, and 202x202. The results indicate that grid independence is achieved on 102x102 resolution.

The following boundary conditions are used. A uniform velocity profile is prescribed at the supply inlet. All wall boundaries are no-slip. At the outlet, the normal derivatives for all variables are set to zero and streamwise velocity must always satisfy global mass conservation.

3. Computational results

The results are presented in two sections: the effects of end-wall opening and the effects of Reynolds number. The details are as follows.

3.1. Effects of end-wall opening

Figure (2), see back page, shows the series of flow patterns for all opening ratios at $Re = 1$. Flow pattern is presented by streamlines, evaluated from the stream function ψ, which is defined as $\psi_i = \psi_{i-1} + \int_{i-1}^{i} u dy$. The value of stream function at each opening ratio is rescaled into range, from 0 to 1, by

$$\psi = \frac{\psi_i - \psi_{MIN}}{\psi_{MAX} - \psi_{MIN}},$$

where ψ_{MIN} and ψ_{MAX} are the minimum and the maximum values of stream function at each opening ratio.

For full opening case, streamlines spread out from the supply inlet and fill up the whole chamber rapidly in the upstream portion, reach uniform distribution in direction along the chamber height slightly before mid length of the chamber, then go straight out of the chamber at the outlet plane. This indicates that the jet from the supply inlet spreads out rapidly and fills up the chamber in the upstream portion, then moves axially downstream and out of the chamber at the outlet.

As the opening ratio decreases, flow pattern in the upstream portion of the chamber changes very little from that of the full opening case; jet spreads out rapidly and streamlines reach uniform distribution in direction slightly before mid length. In the downstream portion of the chamber, however, the upper streamlines near the end-wall curve downwards, then turn and go under the end-wall and out of the chamber. The curvature increases as the end-wall closing increases. This indicates that the flow in this area is bent downwards, then turns and moves under the end wall and out of the chamber.

The details of streamwise velocity profiles are shown in Fig. (3). In the upstream portion, the result shows the wall jet profile at x/L = 0.04 for all openings developing into a fully developed channel profile at x/L = 0.36. Between x/L = 0.36 and 0.68, the profiles stay fully developed. In the downstream portion, the fully developed profiles go through another transformation as the flow moves towards x/L = 0.96 and 1.0 (outlet plane). There, depending upon the end-wall closing, the point of maximum velocity moves downwards towards the lower wall: the more the closing, the further down the location of the maximum velocity. Note that there is no reverse flow throughout the chamber and there is no entrainment of fluid from outside at the outlet plane, i.e., at x/L = 1.0 (see also Fig. 2).

The series of flow pattern at Re = 10 is shown in Fig. (4), see back page. For full opening case, streamlines spread out from the supply inlet and fill up the chamber in the upstream portion similar to case Re = 1, but less rapid due to the existence of a large recirculation region in the lower-left corner under the inlet. Downstream of the recirculation region, uniform distribution in direction of streamlines emerges and goes out of the chamber at the outlet plane.

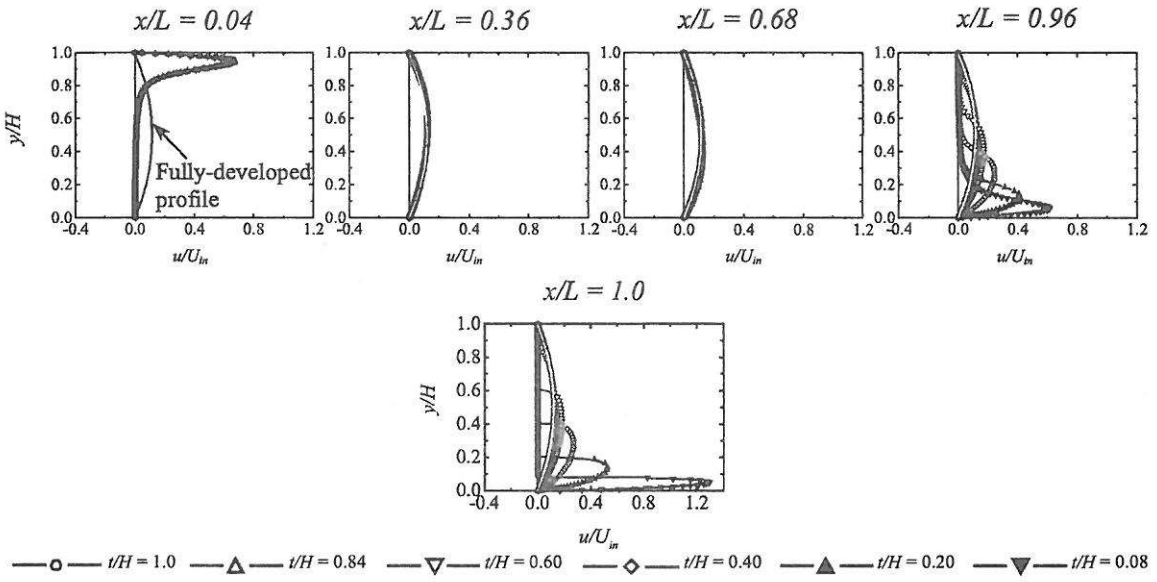

Figure 3. Effect of end-wall opening on streamwise velocity profiles at $Re = 1$.

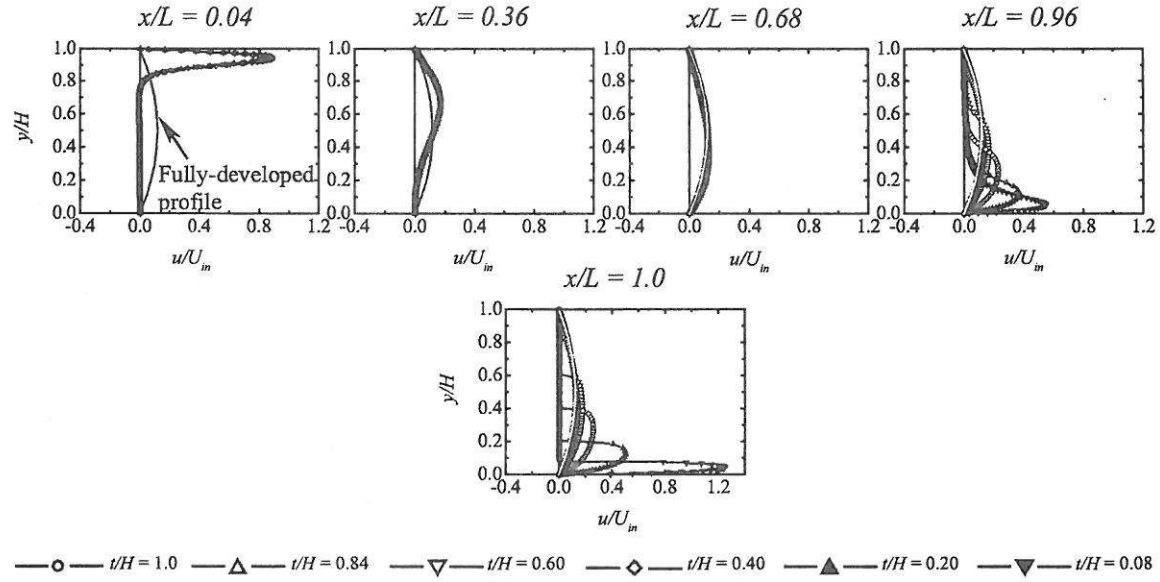

Figure 5. Effect of end-wall opening on streamwise velocity profiles at $Re = 10$.

As the opening ratio decreases, the flow pattern in the upstream portion is nearly unchanged. This can be seen from the pattern of streamlines and the size and the position of the recirculation region. In contrast, the flow pattern in the downstream portion changes gradually with the opening ratio. Specifically, similar to case of $Re = 1$, the upper streamlines near the end wall curve downwards, then turn and go under the end wall and out of the

chamber, with larger curvatures as end-wall closing increases.

The streamwise velocity profiles for case of $Re = 10$ are shown in Fig. (5). For all openings, the wall jet profile at $x/L = 0.04$ develops into the fully-developed channel profile at $x/L = 0.68$, less rapid than what observed in case of $Re = 1$. Then, the profiles further develop as the flow moves downstream towards $x/L = 0.96$ and 1.0; the final profile depends upon the end-wall closing: as in the previous case, the more the closing, the further down the location of the maximum velocity. In addition, the figure clearly shows that the end-wall closing hardly affects the flow in the upstream portion of the chamber but strongly affects the flow in the downstream one, especially near the end wall. Note that there is still no reverse flow and no entrainment of fluid from outside at the outlet plane (see also Fig. 4).

Figure (6), see back page, shows the effects of end-wall opening on flow pattern at $Re = 100$. For this case, the result for additional opening ratio of 0.30 is also shown. For full opening case, the streamlines show wall jet under the ceiling traveling directly from inlet to outlet. As the jet moves downstream, it entrains surrounding fluids in the chamber and carries them out of the chamber through the upper part of the outlet. As a result, the mass flux of fluid carried out of the chamber by the wall jet is more than the mass flux flowing in at the supply inlet. In order to satisfy global mass conservation, the outside fluid is thus entrained into the chamber through the lower part of the outlet. The entrained fluid from outside then moves upwards towards the jet and turns towards the jet direction as it is being entrained into the jet; thus, completing the 'cycle.' As a result, a large recirculation, whose circulation eye stays on the outlet, is formed in the middle of the chamber.

As the end-wall opening decreases from full opening to just above 30%, the flow pattern changes gradually. Wall jet, entraining surrounding fluid in the chamber, detaches from the ceiling and detours downwards under the influence of adverse pressure gradient in front of the end-wall as shown in Fig. (7). The jet then moves under the end wall and out of the chamber on the upper part of the outlet. At the same time, outside fluid is being entrained into the chamber on the lower part by the same mechanism as described previously. The entrainments of chamber fluid by the jet and of outside fluid into the chamber thus form a recirculation region, as before, but now its eye moves downwards and upstream into the chamber as the end-wall closing increases.

It is interesting to note that, if we glance through the flow pattern in this range of openings (full opening to just above 30%), it is much like a backward-facing step flow with the recirculation region extending outside the chamber and, as a result, with the reattachment point located outside. This fictitious view will be proven insightful as we shall see in the Discussion Section.

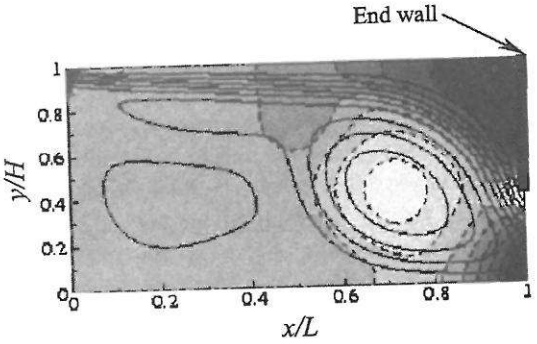

Figure 7. Pressure contours (dotted lines) for case $Re = 100$ and $t/H = 0.40$; Dark color – high pressure, Light color – low pressure. Streamlines are also shown for comparison.

At the approximated end-wall opening of just above 30%, the main recirculation region just moves completely inside the chamber and the reattachment point just lies at the lower corner of the outlet. Entrainment of outside fluid is now stopped, and it can be said that the diverted and detoured wall jet just impinges on the floor inside the chamber (as opposed to outside, by considering the position of the stagnation point).

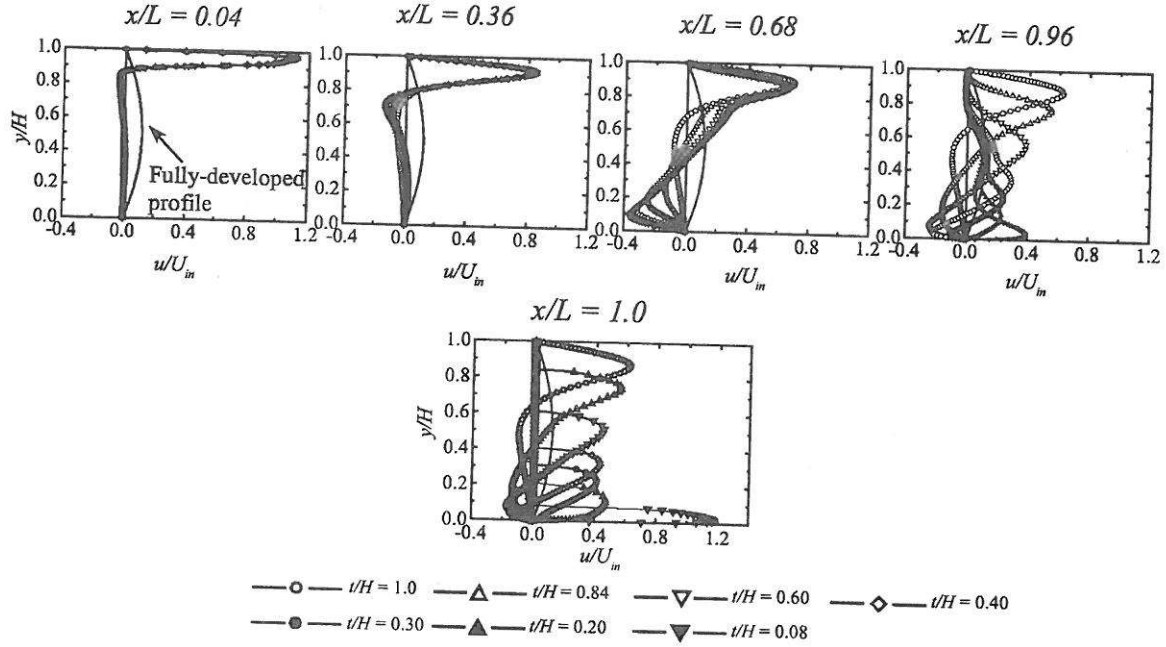

Figure 8. Effect of end-wall opening on streamwise velocity profiles at $Re = 100$.

As opposed to cases of end-wall opening larger than 30%, in the range of end-wall opening less than 30%, flow pattern inside the chamber is nearly unchanged as the opening decreases. In addition, there is an obvious difference between flow patterns in this smaller opening range and the larger one. Namely, the detached wall jet in this range - instead of moving under the end-wall and out of the chamber - is diverted downwards and towards the floor, causing the impingement of the jet and the corresponding reattachment-stagnation point inside the chamber - a feature not observed in the larger opening range and thus shown here by stagnation streamlines. Along the stagnation streamline, the 'jet' is divided into 2 parts. The inner part, after impingement, moves upstream along the floor and forms (another wall jet and) the recirculation region. The outer part moves under the end-wall and out of the chamber, at the same time prohibiting the outside fluid to be entrained into the chamber. Note that here the term 'jet' is loosely referred to a layer of relatively high momentum fluid; hence, it contains both supply fluid and recirculation fluid as the latter is 'entrained' (imparted with vorticity and momentum, in this case, through viscous action) into the jet.

The development of flow pattern at $Re = 100$ can be investigated in more details in the streamwise velocity profiles in Fig. (8). Figure (8) shows that, in the range from full opening to approximately 30%, end-wall opening affects the velocity profiles throughout the chamber, with varying degrees of influence from more in the downstream portion and less in the upstream portion. This is unlike and in contrast to the cases of $Re = 1$ and 10, in which only the very downstream portion is significantly affected. Also, unlike the velocity profiles of $Re = 1$ and 10, those of $Re = 100$ show reverse flow, the recirculation region in the downstream portion, and the entrainment of outside fluid into the chamber through the lower part of the opening (Figs. 6 and 8). However, as the end-wall opening decreases to lower than 30%, the velocity profiles are nearly unchanged, except near the end-wall, and entrainment of outside fluid is now prohibited

in this range. Furthermore, at all opening ratios, the velocity profiles do not approach, or collapse into, a parabolic shape of laminar fully-developed channel flow. This indicates that the chamber length is relatively too short for the jet to develop into fully-developed channel flow state.

3.2. Effects of Reynolds number

To investigate further the influence of Reynolds number, the flow patterns at full opening, 60% and 8% openings of Re = 1, 10, and 100 are compared in Fig. (9), see back page. Figure (9) clearly shows that, at Re = 1 and 10, the flow pattern in the upstream portion for all opening ratios change only as Reynolds number increases while the flow pattern in the downstream portion changes only as opening ratio decreases. This indicates that the Reynolds number influences flow pattern only in the upstream portion of the chamber while the end-wall opening influences only in the downstream one.

As the Reynolds number increases from 10 to 100, the flow pattern changes quite dramatically throughout the chamber. At Re = 10, the recirculation appears in the lower-left corner under the inlet for all opening ratios, while at Re = 100 the recirculation also appears near the outlet and increases in number as the opening ratio decreases. In addition, at Re = 100, for full opening case, wall jet appears under the ceiling; travels from inlet to outlet; and exits through the upper portion of the outlet while outside fluid is being entrained into the chamber through the lower portion of the outlet. As opening ratio decreases to 0.60, wall jet curves downwards gradually and outside fluid is still being entrained into the chamber. Finally at t/H = 0.08, wall jet on the ceiling curves downwards, partly along the end wall, and impinges on the floor, causing the reattachment-stagnation point inside the chamber; and the entrainment of outside fluid into the chamber is now stopped. These results indicate that both Reynolds number and end-wall opening influence the flow pattern throughout the chamber in this range of higher Reynolds numbers.

Finally, it is interesting to note that the recirculation regions in the lower-left corner of Re = 10 and 100 are opposite in direction. The recirculation of Re = 10 is driven by the jet from the supply inlet and rotates in the clockwise direction while that of Re = 100 is driven by reverse flow and rotates in the counter clockwise direction.

4. Discussions

Because the results of this work are complementary to those of S&B (2000), the two studies shall now be discussed to explore further physics of the flow. The results of S&B (2000) are summarized below. However, first note that, in the present study, laminar flow is investigated while in S&B (2000) turbulent flow is investigated. Therefore, it should be emphasized that the interpretation is certainly qualitative in nature and, for turbulent flows, this must be viewed in the sense of mean flow properties.

S&B (2000) studied the effects of supply-air velocity and end-wall opening on temperature distribution inside the ventilated chamber and found that (Fig. 10), at high-supply air velocity (U_{in} = 4.4 m/s, Re = 10,000), the variations of average temperature with end-wall opening for both the upper and lower zones had common characteristics but, at low supply-air velocity (U_{in} = 0.5 m/s, Re = 1,000), they had different characteristics. Namely, at high supply-air velocity, the average temperature in both the upper and lower zones depended upon the closing in the range from 0 (fully open) to δ; beyond δ, the average temperature was relatively independent of the closing. However, at low supply-air velocity, the average temperature in the upper zone exhibited similar characteristic as that was found at high velocity while, in the lower zone, it exhibited linear dependency on the closing throughout the mid 60% range of the closing (t/H from 0.84 to 0.24), even when the closing was beyond δ. In that study, δ is loosely defined as the width of the wall jet at the outlet plane in a fully open case.

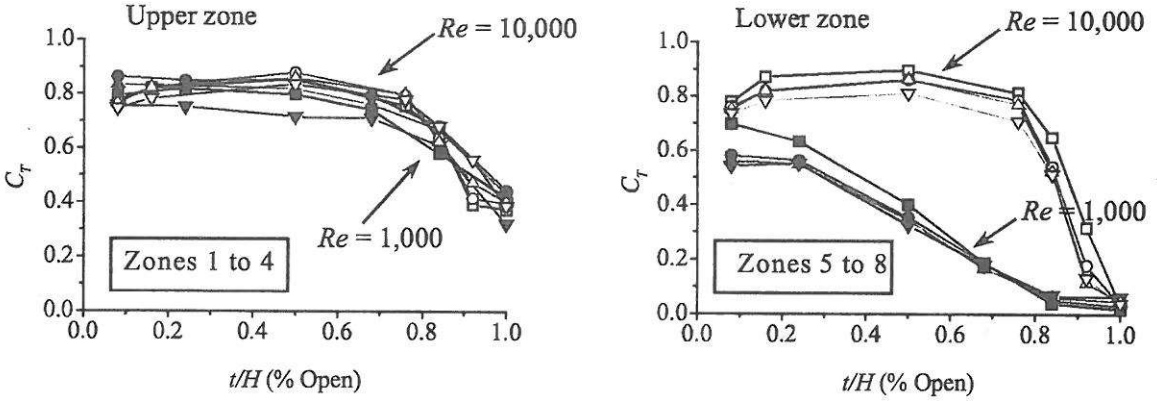

Figure 10. Effects of supply-air velocity on the average temperatures in the upper and the lower zones for case L000; solid symbols – low supply-air velocity (Stitsuwongkul and Bunyajitradulya, 2000), open symbols – high supply-air velocity (Khuhiran et al., 1999). Note that each line represents the data for each zone.

On the other hand, the present results show that, at Re = 100, the flow pattern depends on end-wall closing only in the range from 0 (fully open) to approximately 70% closing (30% opening). In contrast, in the range of end-wall closing more than 70%, the flow pattern is nearly unchanged.

As it is clear, the two results reveal some similar characteristics, albeit some difference in Reynolds number. That is, the flow characteristics depend on the end-wall closing only in the range from 0 to the end-wall closing characteristic height, δ_c. Beyond δ_c, the flow characteristics are relatively independent of the closing. This triggers a key question: What is then the end-wall closing characteristic height, δ_c, that correlates the physics and the observed results? And, if such characteristic length exists, is it applicable to the low velocity case of S&B (2000)? For the latter question, the clue is, in fact, in Fig. (10). From the figure, notice that some independence of the average temperature on end-wall opening is in fact observed in the lower zone as the end-wall opening decreases to below 0.24. But, because there are still few data points in that range, further data or evidence must be sought. Therefore, in order to answer these questions,

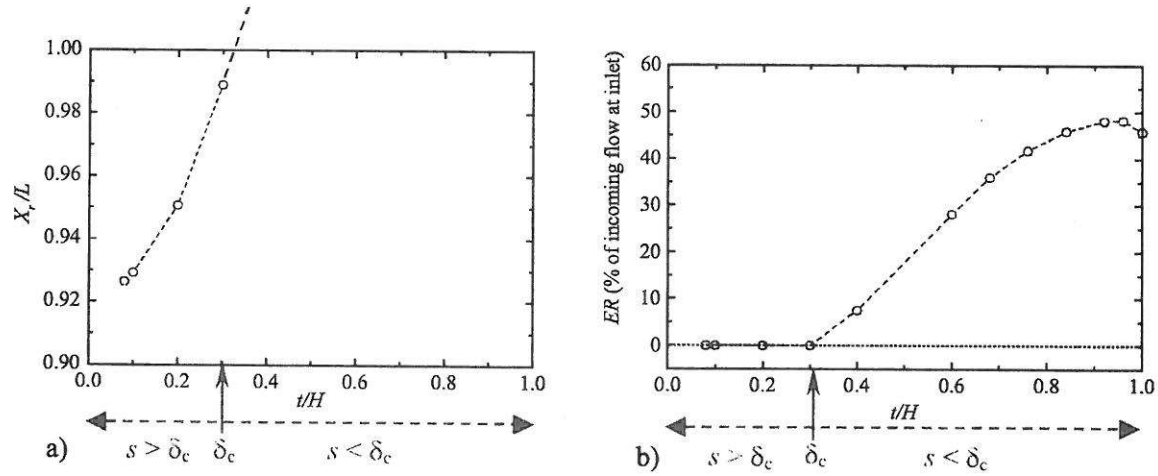

Figure 11. Effects of end-wall closing characteristic height on flow behavior.

the flow characteristics at Re = 100 are investigated in detailed as follows.

The variation of flow characteristics with the end-wall closing (opening ratio) is shown in Fig. (11). Figure 11(a) shows the variation of the reattachment length that is measured from the lower-left corner to the reattachment point and Fig. 11(b) shows the variation of entrainment ratio. The entrainment ratio is defined here as the ratio of the incoming mass flux at the outlet plane to the incoming mass flux at the supply inlet. The results reveal that, as the end-wall closing is less than δ_c, there is no reattachment point inside the chamber and outside fluid is entrained into the chamber. [Note that, in this range of closing, it is useful to think of the reattachment point as locating outside the chamber and moving inwards as the opening decreases, so illustrated by the extended, thick dotted line in Fig. 11a. Equivalently, it is useful to think of the flow pattern (Fig. 6) in this range as a backward facing step flow with the recirculation and the reattachment point extending outside the chamber.] On the contrary, as the end-wall closing is more than δ_c, the reattachment point moves inside the chamber and the outside fluid is no longer allowed to be entrained into the chamber. The flow pattern is nearly unchanged. These results suggest that δ_c is in fact the end-wall closing height that just causes the existence of the reattachment point inside the chamber. In other words, δ_c is the end-wall closing height that initiates the prohibition of outside fluid to be entrained into the chamber.

To further find evidence to support this interpretation of δ_c, smoke-wire flow visualization pictures for the case of low supply-air velocity are therefore studied in Fig. (12), see back plate. These pictures are unpublished flow visualization pictures of Stitsuwongkul (2000). Note that, because of the difficulty in using the technique at high velocity, the low velocity case is therefore investigated. Nonetheless, part of flow visualization evidence for high velocity, using tuft technique, can also be found in Khuhiran et al. (1999). In Fig. (12), except for case t/H = 0.08, there were four vertical wires located along the streamwise direction in the center plane of the chamber. Note that there is one wire near the supply-air inlet, and another one near the outlet. For case t/H = 0.08, there was only one vertical wire near the supply-air inlet. From Fig. (12), for full opening case, the picture depicts smoke *only* on the right hand side (downstream side) of the upper part of each wire, while *only* on the left hand side (upstream side) of the lower part of each. This picture thus depicts a wall jet, moving from inlet to outlet, in the upper part and recirculation in the lower part. In addition, attention should be paid to the fourth wire near the outlet. There, for the lower part of the wire, the fact that smoke is seen only on the left hand side of the wire signifies the direction of air flowing from downstream towards upstream. This clearly indicates that outside air is being entrained into the chamber in the lower part. Furthermore, there is no sign of jet impingement or reattachment point inside the chamber.

As the opening ratio decreases from full opening to approximately 0.50, the wall jet in the upper part of the chamber detours downwards and moves under the end wall and out of the chamber. The outside air is still being entrained into the chamber in the lower part of the chamber. Again, there is no sign of jet impingement and reattachment point inside the chamber.

In contrast, as the opening ratio further decreases to 0.24 and 0.08, flow visualization pictures show different scenario. Specifically, the wall jet is now diverted downwards and impinges on the floor, causing the reattachment point inside the chamber near the outlet. Notice that, unlike previous openings, there is now smoke on *both* sides of the lower part of the fourth wire. Smoke on the left shows the (inner) part of the impinging-jet fluid that is being injected back into the chamber; smoke on the right, the (outer) part being thrown out of the chamber. Outside air is no longer observed to be entrained into the chamber.

In summary, flow visualization reveals that, in the range of end-wall closing less than δ_c, no

obvious jet impingement and the associated reattachment point can be observed inside the chamber, while outside fluid is observed to be entrained into the chamber. On the contrary, in the range of end-wall closing more than δ_c, the opposites are observed. That is, jet impingement and the associated reattachment point is observed inside the chamber, while outside fluid is no longer seen to be entrained into the chamber. Thus, these visualizations have similar characteristics to the computed flows at $Re = 100$ and qualitatively support the interpretation and physics of δ_c. In addition, these results together with the independence of the average temperature on end-wall opening observed for opening ratios less than 0.24 in Fig. (10) suggest that δ_c also exists in the case of $Re = 1{,}000$.

Finally, when these conclusions are applied to the results on average temperature of S&B (2000), they indicate that the reason for variation in average temperature with end-wall opening (Fig. 10) is the dependency of the entrainment ratio on the opening (Fig. 11b). In addition, since outside air is entrained into the chamber through the lower portion of the outlet, the lower zones of the chamber are most affected in comparison to the upper zones.

5. Conclusions

In this study, the characteristics of laminar flow in ventilated chamber are investigated numerically for the effects of end-wall opening and Reynolds number. The study indicates that, at low Reynolds number range, $Re = 1$ and 10, Reynolds number affects the flow pattern only in the upstream portion of the chamber, while the end-wall opening affects the flow pattern only in the downstream portion. On the other hand, at higher Reynolds number range, $Re = 100$, both Reynolds number and end-wall opening affect the flow pattern throughout the whole chamber. In addition, at high Reynolds number, flow pattern and characteristics depend on the end-wall opening only in the range from full opening to just above 30% opening. Below 30% opening, the flow pattern and characteristics are nearly unchanged with end-wall closing. In addition, the independence of the flow pattern and characteristics on end-wall closing is found to be associated with the existence of the reattachment-stagnation point of the impinging jet and the lack of entrainment of outside air.

With these results, the present study extends the physical understanding of flow in ventilated chamber from the study of S&B (2000). Specifically, the study reveals that the flow characteristics in a ventilated chamber depend on the end-wall closing only in the range of closing from 0 (fully open) to the end-wall closing characteristic height, δ_c. Beyond δ_c, the flow characteristics are relatively independent of the closing. From physical considerations, δ_c is found to be the closing height that just causes the reattachment-stagnation point of the impinging jet to exist inside the chamber. Equivalently, δ_c is the closing height that initiates the prohibition of outside fluid to be entrained in to the chamber.

Finally, the results from this study have implications and applications in engineering. Firstly, by using tuft or smoke technique to detect impinging jet and the associated reattachment-stagnation point, or entrainment, it should be convenient enough to find δ_c in some of the real-world applications. Secondly, as for towards future research and for ease of engineering applications, the correlation for δ_c or between δ and δ_c is desired. Specifically, the non-dimensional correlation $\delta_c/h = f(Re, L/H, h/H)$ or $\delta_c/\delta = f(Re, L/H, h/H)$ is desired, where δ is loosely defined at this point to be the characteristic thickness of the ceiling wall jet at the exit plane in fully-open case. The reason for still using δ in the second functional form is partly because there are already available data for the growth and decay of a wall jet (e.g., Launder and Rodi, 1981); partly because it is physically easy to grasp; and partly because in some applications in which the end-wall closing is to be fixed, some check point measurement can be made.

References

[1] Armaly, B.F., Durst, F., Pereira, J.C.F., and Schonung, B., (1983), "Experimental and Theoretical Investication of Backward -Facing Step Flow," *J. Fluid Mech.*, Vol. 127, pp. 473-496.

[2] Davidson, L. and Nielsen, P.V., (1996), "Large Eddy Simulations of The Flow in a Three-dimensional Ventilated Room," In *The 5th Int. Conf. On Air Distributions in Rooms, ROOMVENT'96*, July 17-19, Vol. 2, pp. 161-168, Yokohama, Japan.

[3] Davidson, L., Nielsen, P.V., and Topp. C., (2000), "Low-Reynolds Number Effects in Ventilated Rooms: A Numerical Study," In *The 7th Int. Conf. On Air Distributions in Rooms, ROOMVENT 2000*, pp. 307-312, Reading, U.K.

[4] Ghia, U., Ghia, K.N., and Shin, C.T., (1982), "High-Re solutions for incompressible flow using the Navier-Stokes equations and a multigrid method," *J. Comput. Phys.*, Vol. 48, pp. 387-411.

[5] Gosman, A.D., Nielsen, P.V., Restivo, A., and Whitelaw, J.H., (1980), "The Flow Properties of Rooms With Small Ventilation Openings," *J. Fluids Eng.*, Vol. 102, pp. 316-323.

[6] Khuhiran, C., Mantajit, J., Wetchagarun, S., Boonrat, S., Katsuwon, T., Stitsuwongkul, T., and Bunyajitradulya, A., (1999), "Effect of End-Wall Opening on Temperature Distribution in A Ventilated Chamber," Proceeding of The Thirteenth National Mechanical Engineering Conference, Vol. 1, pp. 9-16.

[7] Launder, B. E., and Rodi, W., (1981), "The Turbulent Wall Jet," *Prog. Aerospace Sci.*, Vol. 19, pp. 81-128.

[8] Nielsen, P.V., Restivo, A., and Whitelaw, J.H., (1978), "The Velocity Characteristics of Ventilated Rooms," *J. Fluids Eng.*, Vol. 100, pp. 291-298.

[9] Restivo, A., (1979), "Turbulent Flow in Ventilation Rooms," Ph.D. Thesis, Mechanical Engineering Department, Imperial College of Science and Technology.

[10] Stitsuwongkul, T., (2000), "Mixing Enhancement in a Ventilated Chamber by Means of Manipulation of a Nozzle Exit," M. Thesis, Department of Mechanical Engineering, Faculty of Engineering, Chulalongkorn University.

[11] Stitsuwongkul, T., and Bunyajitradulya, A., (2000), "Temperature Distribution Inside A Ventilated Chamber: Effects of Lobed Nozzle, Supply-Air Velocity, and End-Wall Opening," Research and Development Journal of The Engineering Institute of Thailand, Vol. 11, No. 3, pp. 57-68.

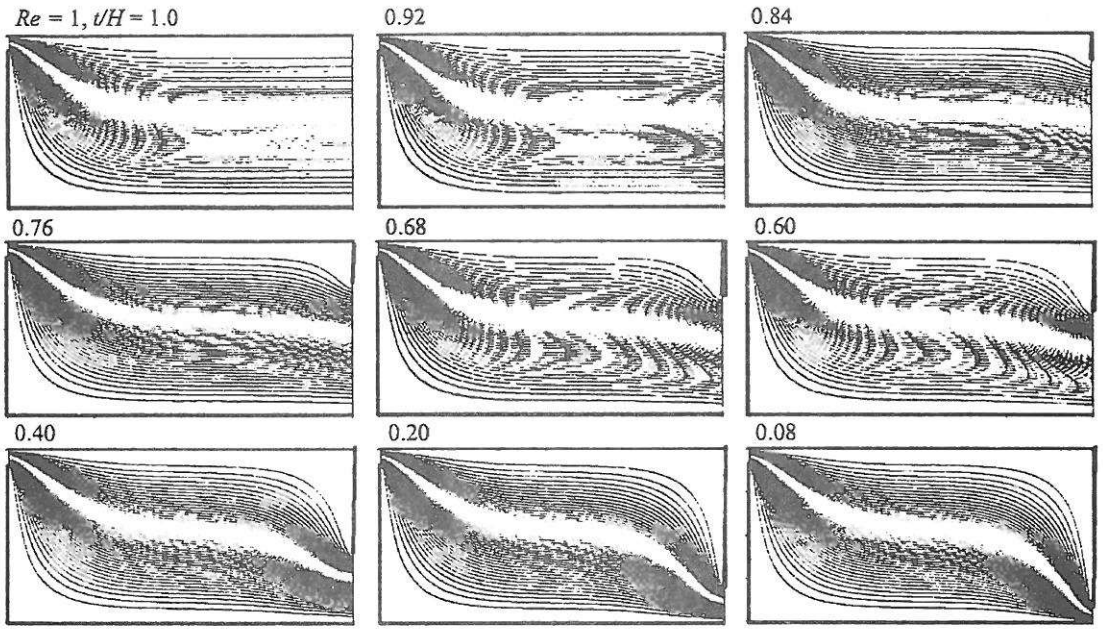

Figure 2. Effects of end-wall opening on flow pattern at $Re = 1$.
(Thick line at the end represents the end-wall.)

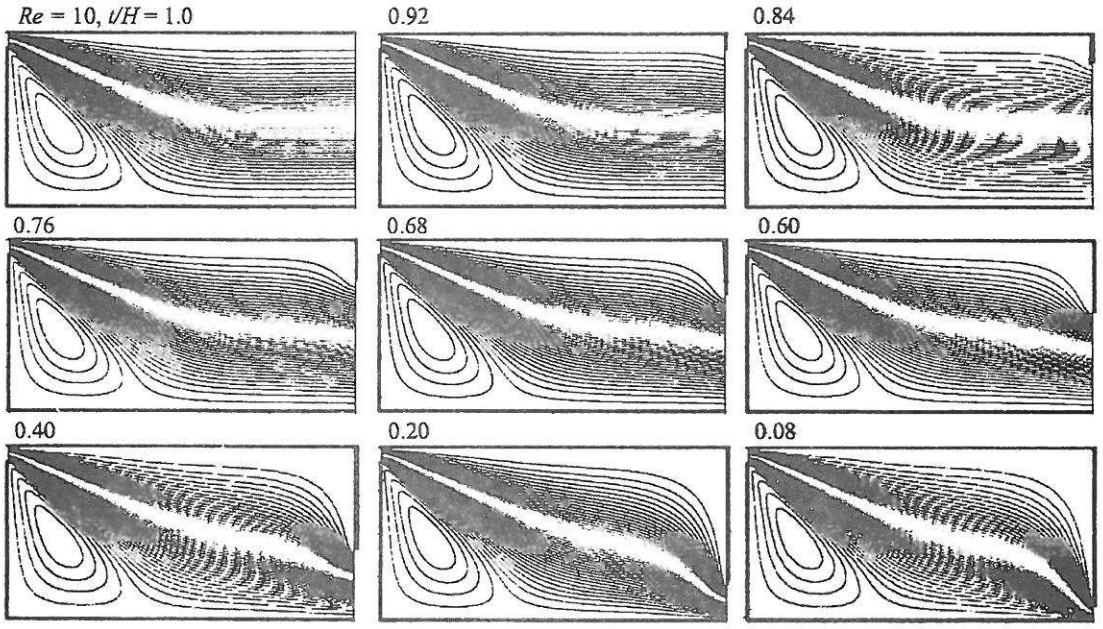

Figure 4. Effects of end-wall opening on flow pattern at $Re = 10$.
(Thick line at the end represents the end-wall.)

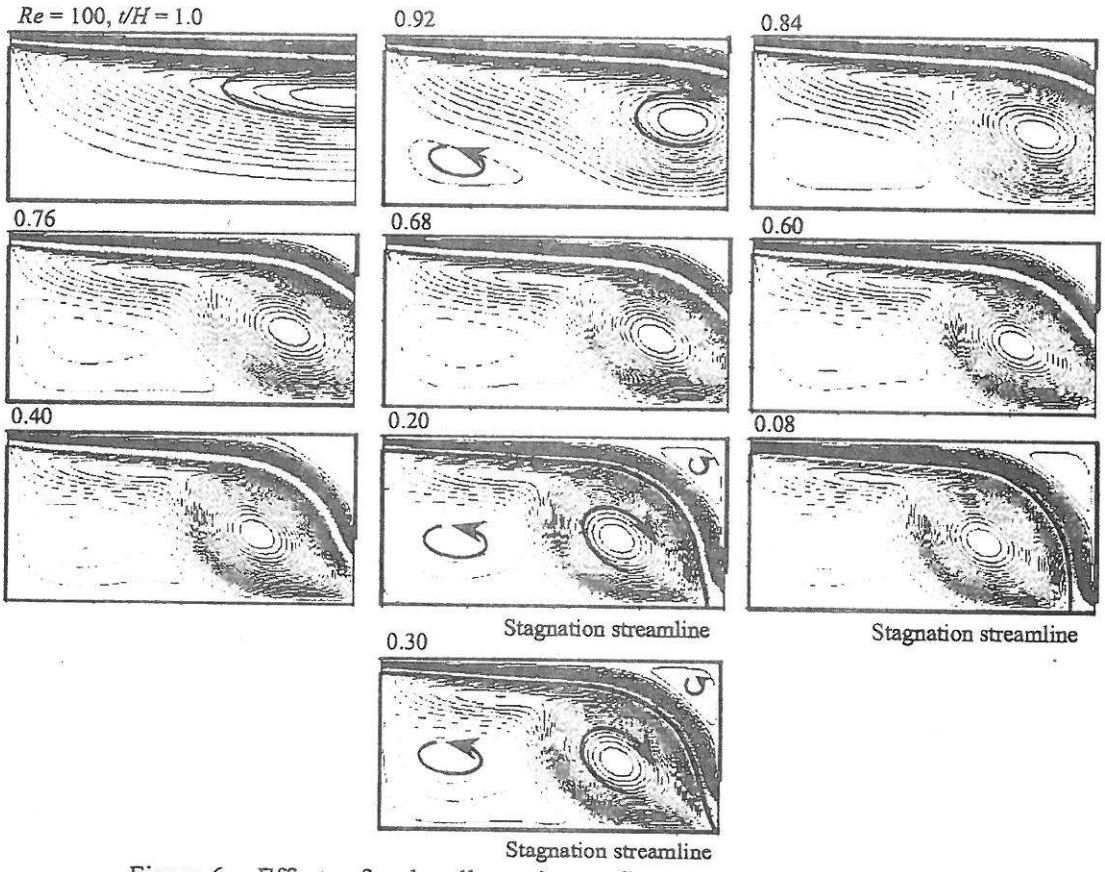

Figure 6. Effects of end-wall opening on flow pattern at $Re = 100$.
(Thick line at the end represents the end-wall.)

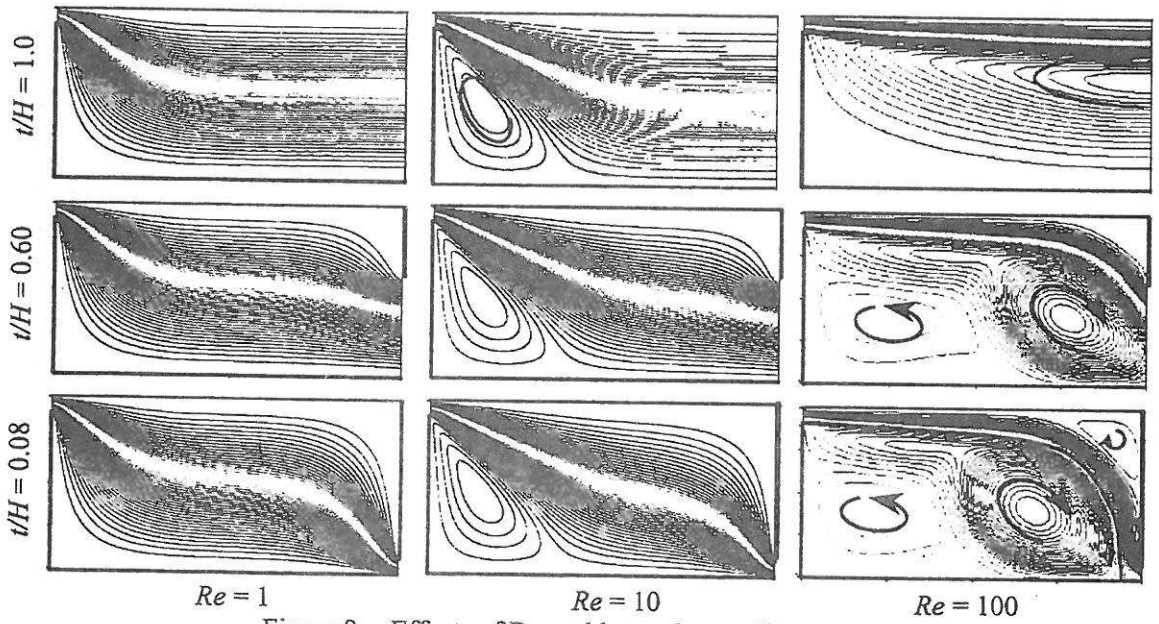

Figure 9. Effects of Reynolds number on flow pattern.
(Thick line at the end represents the end-wall.)

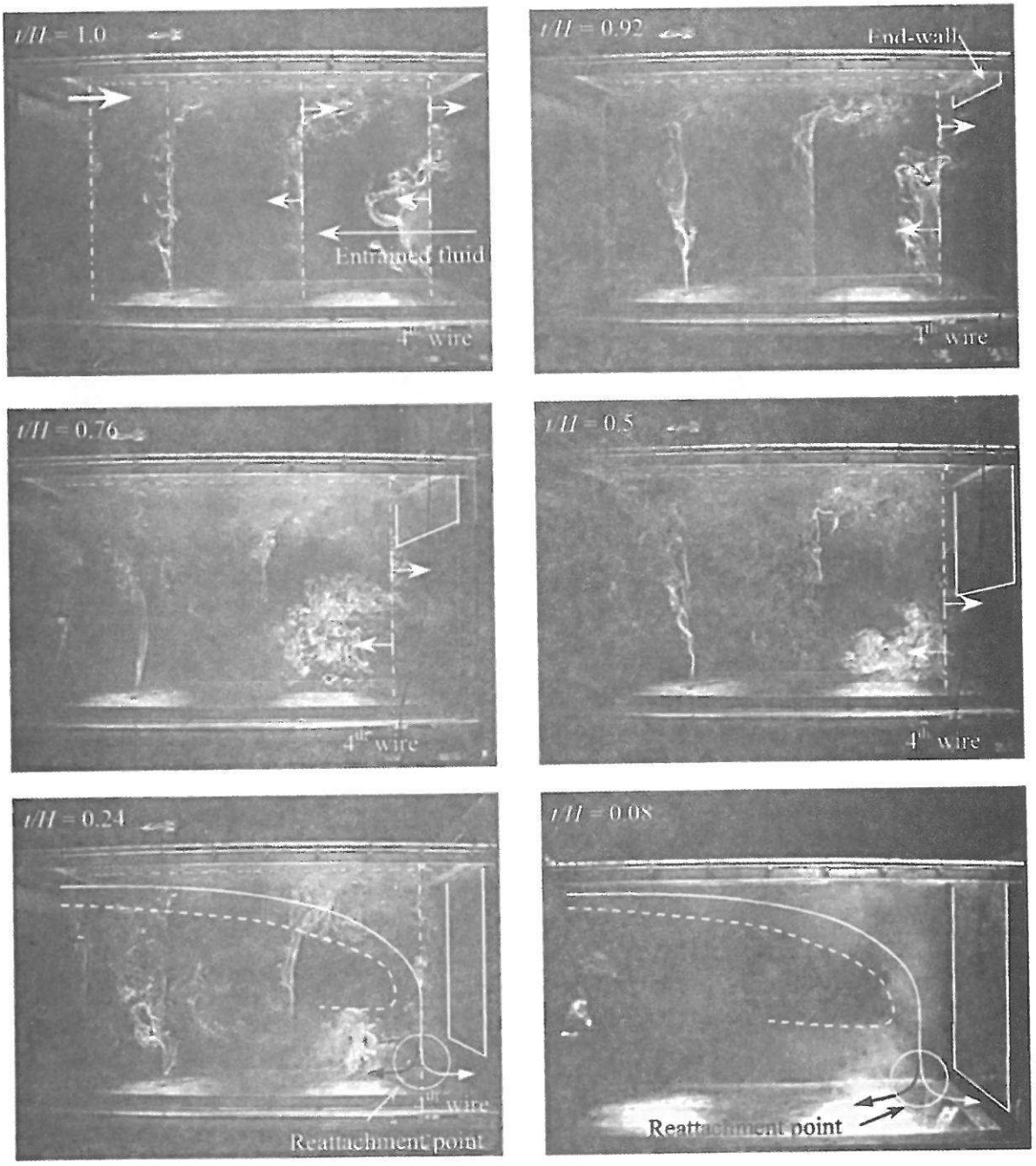

Figure 12. Smoke-wire flow visualization, *Re* =1,000(Stitsuwongkul, 2000).